Advances in Nano Research, *Vol. 15, No. 5 (2023) 385-399*
https://doi.org/10.12989/anr.2023.15.5.385

Edge perturbation on electronic properties of boron nitride nanoribbons

K.L. Wong, K.W. Lai, M.W. Chuan, Y. Wong, A. Hamzah, S. Rusli,
N.E. Alias, S. Mohamed Sultan, C.S. Lim and M.L.P. Tan*

Faculty of Electrical Engineering, Universiti Teknologi Malaysia, 81310 Skudai, Johor, Malaysia

(*Received October 27, 2020, Revised October 10, 2023, Accepted October 17, 2023*)

Abstract. Hexagonal boron nitride (h-BN), commonly referred to as Boron Nitride Nanoribbons (BNNRs), is an electrical insulator characterized by high thermal stability and a wide bandgap semiconductor property. This study delves into the electronic properties of two BNNR configurations: Armchair BNNRs (ABNNRs) and Zigzag BNNRs (ZBNNRs). Utilizing the nearest-neighbour tight-binding approach and numerical methods, the electronic properties of BNNRs were simulated. A simplifying assumption, the Hamiltonian matrix is used to compute the electronic properties by considering the self-interaction energy of a unit cell and the interaction energy between the unit cells. The edge perturbation is applied to the selected atoms of ABNNRs and ZBNNRs to simulate the electronic properties changes. This simulation work is done by generating a custom script using numerical computational methods in MATLAB software. When benchmarked against a reference study, our results aligned closely in terms of band structure and bandgap energy for ABNNRs. However, variations were observed in the peak values of the continuous curves for the local density of states. This discrepancy can be attributed to the use of numerical methods in our study, in contrast to the semi-analytical approach adopted in the reference work.

Keywords: BNNRs; edge perturbation; electronic properties; Green's function; Hamiltonian matrix; nearest neighbor; tight binding model

1. Introduction

Hexagonal boron nitride nanoribbons (h-BNNRs) is a chemical compound analogue to graphene nanoribbons (GNRs) (Zeng *et al*. 2010) that consist of two edge orientations, which are Armchair edge and Zigzag edge with honeycomb lattice (DiBenedetto and Khatun 2018). h-BN produced by hot pressing, with the material being slightly hygroscopic and machinable with conventional tooling (Morrell 2000). h-BN, also called as white graphene can be produced by Chemical Vapour Deposition (CVD) (Kumar and Pattammattel 2017). BNNRs possess a higher thermal stability, oxidation stability up to 800°C, inert to chemical and good optical properties. The boron atoms and nitrogen atoms in the structure of boron nitride connected with strong covalent bond. However, the interlayer between the boron nitride layers held together with weak Van der Waals force (Song *et al*. 2010).

Boron nitride is a wide band gap semiconductor with the range of 4.3 eV until 6 eV. This is due to edge type and the shape of BNNRs do not cause any changes on energy gap. The spatial separation of electrons and holes make this wide energy band gap (Guerra *et al*. 2019). The properties of band edge can be categorized into direct or indirect in nature. It can be known by measuring exciton-related luminescence and absorption near the edge (Watanabe *et al*. 2004). Hence, a lot of engineering techniques required to change the electronic properties of boron nitride including edge perturbation, addition of defects, doping, surface modifications and other engineering techniques (Lim *et al*. 2017).

Hexagonal boron nitride formed by stacking multiple layer of BNNRs and named as bilayer BNNRs. Boron nitride nanoribbons formed by cutting the strip out from a boron nitride nanosheets (BNNSs) (DiBenedetto and Khatun 2018) as shown in Fig. 1. The red lattice point denoted nitrogen atom whereas the green lattice point denoted boron atom. The number of ribbon width influenced by the number of sub band. The number of sub band is increasing with the number of width.

There are two type of edge orientation of BNNRs, which are Armchair BNNRs and Zigzag BNNRs. ABNNRs has a non-magnetic semiconducting behavior without depends on their width, whereas ZBNNRs perform two characteristics, which are magnetic or non-magnetic based on their edge passivation (Huang *et al*. 2012). The geometry structure of a *N*-ABNNRs is demonstrated in Fig. 2, where *N* represents the width. Similar to Fig. 1, the red lattice points correspond to nitrogen atoms, while the green lattice points denote boron atoms.

The electronic properties of this BNNRs is based on its width (Izyumskaya *et al*. 2017). ABNNRs consists of three families, which are $3p$, $3p + 1$, $3p + 2$. The p is the positive integer. Armchair BNNRs exhibit typical direct gap oscillation with distinct family behavior. The minimization of the edge formation can be done by hydrogen modification of BNNRs. It also can induce significant changes in magnetic and electronic properties, which remain ABNNRs non-magnetic semiconductor.

*Corresponding author, Ph.D.,
E-mail: michael@utm.my

ISSN: 2287-237X (Print), 2287-2388 (Online)

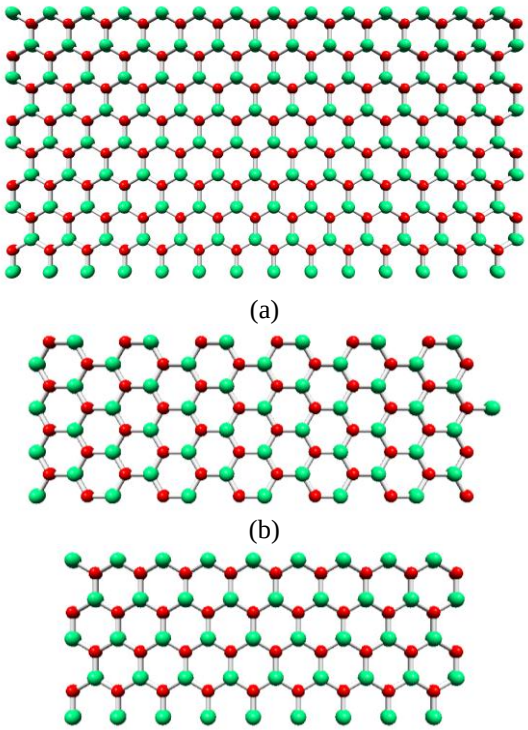

Fig. 1 The configurations of cutting strip of (a) BNNSs into (b) ABNNRs and (c) ZBNNRs

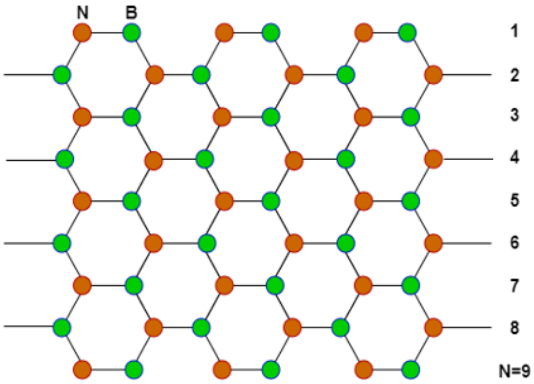

Fig. 2 ABNNRs edge structure with *N*-dimers

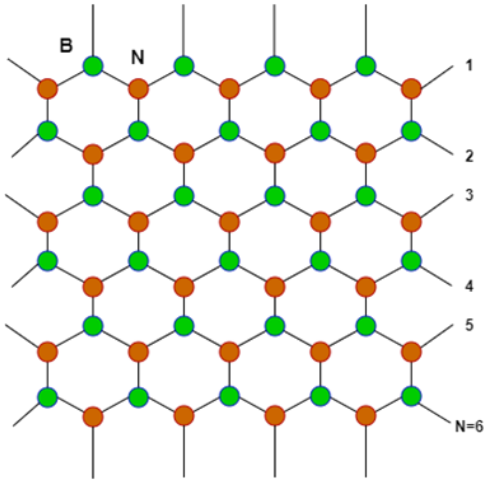

Fig 3 ZBNNRs edge structure with *N*-dimers

The geometry structure for *N*-ZBNNRs is shown in Fig. 3, where *N* represented as width. The orange colour lattice represent the nitrogen atom whereas the green colour lattice point represent the boron atom. One edge of ZBNNRs is more negatively charged and the other edge is more positively charged, this is responsible for the electronegativity of nitrogen and the electropositivity of boron (DiBenedetto 2017). Hydrogen modification of ZBNNRs can display half-metallicity and become ferro-magnetic metals with either hydrogen termination only at the B-edge or full surface hydrogenation. The energy gap of ZBNNRs is decreases monotonically with ribbon width increasing, although the electronic structure of ZBNNRs is not spin-polarized (Zheng *et al*. 2009). Tight binding is similar to Linear Combination of Atomic Orbitals (LCAO), it is a method used to calculate the electronic band structure of a crystal (Wong *et al*. 2019; Chimalgi *et al*. 2014). The tight binding method can be worked by recording the Hamiltonian's eigenstates in an atomic-like basis set, and replaced the parameterized Hamiltonian matrix by the exact many-body Hamiltonian operator (Goringe *et al*. 1997).

2. Literature review

2.1 Introduction

This research used a tight-binding model to investigate the electronic properties of BNNRs. The edge of the BNNRs is being perturbed to study its electronic properties. The solution of Schrödinger's Eq., Hamiltonian Matrix, is used to investigate that particular structure, where the Hamiltonian matrix used defined according to the tight-binding model . The DOS can be calculated by using the band structure to comprehend the energy states occupied in the system. This determination can be achieved using two methods: the mathematical delta function and Green's Function Theory (Datta 2005). With the comprehensive understanding derived from this study, we are poised to make significant strides towards the development of nanotransistors in the future (Chuan *et al*. 2020b).

2.2 History of Boron Nitride (BN)

BN is a chemical compound that consists of boron-nitrogen covalent bonds. The structure of a cubic form of BN (c-BN) is a diamond-like crystalline arrangement, and the bulk crystal of the hexagonal form of BN (h-BN) is analogous to graphite crystal. The 2-dimensional sheets of h-BN are soft among its polymorphs and most stable. The bonding in h-BN is less covalence and higher ionic character. This makes it becomes the best proton conductor. It has the highest thermal conductivity among all the electrical insulators (Kumar and Pattammattel 2017).

h-BN produced by hot pressing, with the material being slightly hygroscopic and machinable with conventional tooling (Morrell 2000). Furthermore, h-BN, also called white graphene can be produced by Chemical Vapour Deposition (CVD). CVD is a bottom-up chemical deposition method used to construct high-quality nanoscale films. Nanolayers of h-BN usually exhibit chemical inertness,

high optical transparency, and thermal stability. Therefore, h-BN leads to finding out atomic layers of other elements such as transition metal dichalcogenides (TMD) with tunable properties (Kumar and Pattammattel 2017).

2.3 Tight-binding model

Tight-binding is similar to the Linear Combination of Atomic Orbitals (LCAO); it is used to calculate the electronic band structure of a crystal. The tight-binding method can be worked by recording the Hamiltonian's eigenstates in an atomic-like basis set and replaced the parametrized Hamiltonian matrix by the exact many-body Hamiltonian operator (Goringe *et al*. 1997).

The tight-binding model is a standard way to get the energy band structures and get the Hamiltonian matrix elements. However, it is not correct for the calculation. Huckel theory needs to be used for the tight-binding model. This is because this theory restricts all interactions to nearest neighbours for a specific set of atomic orbitals. It also helps to minimize the number of atomic orbitals through some approximations (DiBenedetto 2017).

The tight-binding Hamiltonian method required two developments to reduce the energy of atomic configurations. Firstly, the total energy of the system is not the addition of eigenvalues or band energy. This form of total energy has been proved to be the most useful for transition metals in tight-binding calculations. Secondly, a recommendation for getting the force on an atom is created. The most straightforward scheme is to differentiate the constraint from the total DOS to conserve the total number of electrons. This can be completed by numerical differentiation, including the local DOS. This method can compare the local DOS before and after an atomic displacement that can affect at all sites. It is known that many atoms can be effected within the range of Hamiltonian. Writing the band energy as the trace of the product of the density matrix and Hamiltonian is a more efficient way. The product of the density matrix and the derivative of Hamiltonian can be recognized as the derivative of the band energy (Sutton *et al*. 1988).

2.4 Electronic properties of BNNRs

Single-layer (BN) is two-dimensional (2D) crystals. BN always displays special characteristics because of the large iconicity of B and N atoms. ABNNRs have a non-magnetic semiconducting behaviour without depends on their width, whereas ZBNNRs perform two characteristics, which are non-magnetic or magnetic based on their edge passivation (Huang *et al*. 2012). The edge type and the shape of BNNRs do not cause any changes to the energy gap, as it is an insulator with wide band haps (Eg > 4.0eV). The spatial separation of electrons and holes makes this wide energy bandgap (Guerra *et al*. 2019).

For the ABNNRs, the ground states are non-magnetic due to the dangling bonds are inactivated. The average edge energy of ABNNRs shows that it is weak width dependence, where the value is 0.76eV/Å, and lower compared with armchair graphene nanoribbons (AGNRs). The edge stress of ABNNRs oscillates weakly when ribbon width increasing and shows a negative value (-0.26eV/Å).

For the ZBNNRs, the non-magnetic edge stress shows a positive value (0.64eV/Å) because ZBNNRs are under intrinsic tensile stress. The non-magnetic edge energy is unlike ABNNRs, which it does not depend on the ribbon width. The ground states of ZBNNRs are ferromagnetic spin ordering at the N-edges and spin-polarized with antiferromagnetic spin ordering at B-edges (Huang *et al*. 2012).

2.5 Edge perturbation

Edge perturbation serves to introduce an imperfect structure to BNNRs. The BNNRs' structure is inherently delicate and susceptible to defects, which are often inevitable during fabrication. Various techniques, including edge doping, application of stress or strain, among others, can be employed to achieve edge perturbation (DiBenedetto 2017).

2.6 Related work

The structural and electronic properties of ZBNNRs and ABNNRs are studied by using first-principle spin-polarized total energy calculation and modified third NNTB approximation (Chegel 2016). The results showed that the energy gap of ZBNNRs is indirect and decreased gradually when ribbon width increased due to the existence of strong edge states. For ABNNRs, direct bandgap oscillation is exhibited when the width increases due to the presence of very weak edge states (Park and Louie 2008).

The carbon atom substitution can induce the spontaneous magnetization for either boron atom or nitrogen atom of BNNRs (Du *et al*. 2007). The stability of BN bilayers is investigated to determine its ground state energies and interlayer distance using DFT. The hopping parameters and onsite energies extracted using the minimal tight-binding model (Ribeiro and Peres 2011).

Furthermore, a 3-dimensional CBBNs is investigated and studied using first-principle calculations and a tight-binding model. The result showed that the bandgap of CBBNs has a similar variation when BNNRs is increasing in size. The bandgap also limited by the second-neighbour interaction between sp^2-bonded atoms and p_z states in adjacent nanoribbons (Lee and Jhi 2015).

Ab initio linear combination of the pseudoatomic-orbitals method used to calculate the band structure of h-BN. The calculated band structure shows that it had an indirect bandgap insulator and two empty interlayer bands. The DOS is compared with the experimental x-ray emission spectra of boron and nitrogen edges (Ma *et al*. 1993). Truncated crystal approach and periodic small cluster calculation are used to investigate the electronic properties and band structure of hexagonal boron nitrides such as different bandwidths, work function, cohesion energy, and the energy of band-to-band transition. The results are compared with tight-binding, experimental optical, and thermochemical data (Zunger 1974).

Ballistic thermoelectric properties of BNNRs are simulated by using the NEGF atomistic simulation of electron and phonon transport. A result showed that the thermoelectric properties of BNNRs had a smaller thermal conductance and higher power factor (Xie *et al*. 2013). The

strain effects on the electronic properties of BNNRs are investigated by using first-principle calculations. The energy gap for ABNNRs and ZBNNRs decreased as the strain increased (Jin *et al*. 2010).

The analytical study of electronic properties BNNSs including dispersion relation, the DOS, onsite energy, and the hopping integral is carried out using the NNTB model. The results showed that the bandgap is affected by the onsite energy, whereas the shape of the band structure is affected by the hopping integral (Lim *et al*. 2017). The charge redistribution of π electrons is related to the modification of onsite energies. This can be achieved by decorating the edges of nanoribbons using different functional groups (Zhao *et al*. 2010).

The defects of the optical spectra of h-BN are investigated using many-body perturbation theory. The prototypical defects, including isolated boron and nitrogen vacancies, substitutional theory, and the divacancy are embedded into BNNSs (Attaccalite *et al*. 2011). The half metallicity in the ZBNNRs is revealed using Hubbard-type Coulomb interaction (Zheng *et al*. 2009) and first-principles calculations within local spin-density approximation. The ribbon showed a large spin splitting when the boron edge of ZBNNR is passivated (Zheng *et al*. 2008).

The BNNRs is terminated with a few atoms, including fluorine, chlorine, oxygen, sulphur, and phosphorus atom. The DOS and energy band structure are studied after termination using a tight-binding model with extended Huckel Theory. The results showed that semiconducting properties are produced when doped with fluorine and chlorine, whereas metallic properties are produced when doped with oxygen, sulphur, and phosphorus (DiBenedetto and Khatun 2018). The edge of ABNNR is terminated with hydroxide-group results in a polyol-like structure with fringes of hydroxide-groups terminating the two ribbon edges (Lopez-Bezanilla *et al*. 2012).

Carbon chain-doped ZBNNRs is investigated by using first-principles calculations within the local spin-density approximation. The results showed that half-bare ZBNNRs with hydrogen-passivated boron edge and bare carbon edge had a spin-polarized ground state with the ferromagnetic spin ordering localizes at the carbon edge (Tang and Cao 2010).

From previous researchers, they used other model description, including DFT, first principal calculation, and ab initio calculation to compute the electronic properties of BNNRs, which may lead to computationally expensive and time consumed. Next, the edge functionalization techniques used, including doping, addition of defects and vacancy may have a high average roughness on the surface of BNNRs (Chuan *et al*. 2020a). Thus, edge perturbation is introduced to investigate the electronic properties of BNNRs.

3. Research methodology

3.1 Overview

For this research, a basic model of BNNRs developed which the band width and the band length is adjustable by any positive integer. This research used NEGF tight binding model with device modelling simplifying assumptions including basis function, its interaction and the discretization of Hamiltonian into matrix form. The Schrödinger's Eq. (Schrödinger 1926) in a computational method using matrix is done on this research. The Hamiltonian operator, H, of the Schrödinger Eq. accurately describes the physical structure of the device, (Baggott 2000) indicating the position of constituent particles and their interactions with each other. This research focused on the edge perturbation into the top-edge atom and bottom-edge atom of ABNNRs and ZBNNRs respectively by using MATLAB software.

The range of edge perturbation set to be from +3 eV until -3 eV and applied on the respective atom of ABNNRs and ZBNNRs. The hoping integral between neighboring π-orbital of boron nitride atoms or between unit cells is suggested to be 3.01834eV as mentioned in the reference work (DiBenedetto 2017). The collapse of the width direction into single matrix form is done on the decomposition of quasi-2D BNNRs structure into 1D structure. This defined as alpha matrix, whereas the interaction between the alpha matrixes defined as beta matrix. The number of boron-nitride atoms present in BNNRs unit cell equals to the number of rows in alpha and beta matrix. This alpha matrix and beta matrix used to investigate the band structure of ABNNRs and ZBNNRs respectively.

Another MATLAB script is created aside from the construction of Hamiltonian operator. It compute the energy-eigenvalues calculation, plotting of sub-band, local DOS, bandgap value and Green's Function DOS with the input of band width and band length obtained from the main script. The simulation result including band structure shape, numbers of bands on the sub-band plot, local DOS curve plot shape, bandgap energy analyzed and compared with a benchmark reference work (DiBenedetto 2017).

3.2 Generation of Hamiltonian matrix

The Hamiltonian Operator is based on the formation of unit cell, named as alpha (α) and the interaction between the unit cell, named as beta (β) (Goh *et al*. 2018, Chuan *et al*. 2022, Chuan *et al*. 2023). The structure arrangement can be adjusted by using a few parameters, including the width of BNNRs, *n*, length of BNNRs, *l*, edge orientation and edge perturbation. The simulation results of electronic properties are done by using MATLAB software. The output from the MATLAB simulation is the sub-band structure, local DOS, bandgap energy and Green's Function DOS with input parameter. A few terms needed for the generation of 1D Hamiltonian operator including self-interacting energy, ε, and the interaction energy, t replaced with the defined terms, which are α and β in this work. An excerpt of the MATLAB script used for this purpose can be found in the Appendix.

3.2.1 Alpha, α

Alpha matrix is representing the self-interacting unit cells that connecting edge-to-edge in the BNNRs unit cell. A clockwise sequence needed for the numbering of the boron-nitride atoms in the ABNNRs structure. Both off-diagonals are filled for the generation of alpha matrix. A 4-

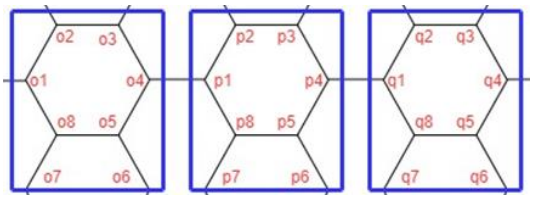

Fig. 4 4-ABNNRs with length=3. Unit cell is highlighted

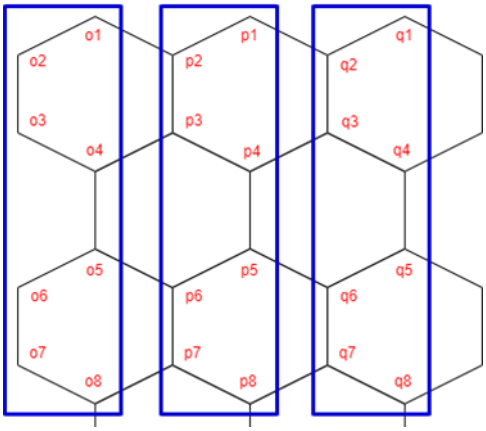

Fig. 5 4-ZBNNRs with length=3. Unit cell is highlighted

ABNNRs with length of 3 took into consideration as shown in Figure.

Each π-orbital connected between atoms in a unit cell represented by t term in the alpha matrix. Staring from 4-ABNNRs, an extra t term is included in the alpha matrix. This is due to the certain π-orbital have 3 nearest neighbor atom bonding within the unit cell. This phenomena reflected in the numbered 5 and 8 atom in the unit cell p. The Eq. (1) shows the alpha matrix Eq. for 4-ABNNRs structure as shown in Fig. 4.

$$\alpha_{4-ABNNRs} = \begin{bmatrix} \varepsilon_B & t & 0 & 0 & 0 & 0 & 0 & t \\ t & \varepsilon_N & t & 0 & 0 & 0 & 0 & 0 \\ 0 & t & \varepsilon_B & t & 0 & 0 & 0 & 0 \\ 0 & 0 & t & \varepsilon_N & t & 0 & 0 & 0 \\ 0 & 0 & 0 & t & \varepsilon_B & t & 0 & t \\ 0 & 0 & 0 & 0 & t & \varepsilon_N & 0 & 0 \\ 0 & 0 & 0 & 0 & 0 & 0 & \varepsilon_B & t \\ t & 0 & 0 & 0 & t & 0 & t & \varepsilon_N \end{bmatrix} \quad (1)$$

For the alpha matrix formation of ZBNNRs, a 4-ZBNNRs with length of 3 took into consideration as shown in Fig. 5. There are 4 boron atoms and 4 nitrogen atoms accordingly, thus 7 π orbitals are formed within a unit cell.

The unit cell of ZBNNRs highlighted using blue colour as shown in Fig. 2. The formation of alpha matrix is straightforward and simple. The t term in the alpha matrix shown in Eq. (2) is the π-orbital between the atoms in the unit cell p.

$$\alpha_{4-ZBNNRs} = \begin{bmatrix} \varepsilon_B & t & 0 & 0 & 0 & 0 & 0 & 0 \\ t & \varepsilon_N & t & 0 & 0 & 0 & 0 & 0 \\ 0 & t & \varepsilon_B & t & 0 & 0 & 0 & 0 \\ 0 & 0 & t & \varepsilon_N & t & 0 & 0 & 0 \\ 0 & 0 & 0 & t & \varepsilon_B & t & 0 & 0 \\ 0 & 0 & 0 & 0 & t & \varepsilon_N & t & 0 \\ 0 & 0 & 0 & 0 & 0 & t & \varepsilon_B & t \\ 0 & 0 & 0 & 0 & 0 & 0 & t & \varepsilon_N \end{bmatrix} \quad (2)$$

3.2.2 Beta, β

A beta matrix represent the interaction between the alpha matrixes, which is the interaction site for π-orbital between the unit cells. The t term in the beta matrix Eq. represent the interaction energy between both unit cells in ABNNRs. For the formation of beta matrix between the unit cell o and unit cell p of ABNNRs is shown in the Eq. (3).

$$\beta_{4-ABNNR} = \begin{bmatrix} 0 & 0 & 0 & 0 & 0 & 0 & 0 & 0 \\ 0 & 0 & 0 & 0 & 0 & 0 & 0 & 0 \\ 0 & 0 & 0 & 0 & 0 & 0 & 0 & 0 \\ t & 0 & 0 & 0 & 0 & 0 & 0 & 0 \\ 0 & 0 & 0 & 0 & 0 & 0 & 0 & 0 \\ 0 & 0 & 0 & 0 & 0 & 0 & t & 0 \\ 0 & 0 & 0 & 0 & 0 & 0 & 0 & 0 \\ 0 & 0 & 0 & 0 & 0 & 0 & 0 & 0 \end{bmatrix} \quad (3)$$

The relationship of other side of the alpha matrix of ABNNRs can be done by transposing the original beta matrix in the Eq. (3). The transposed beta matrix of ABNNs is shown in the Eq. (4).

$$\beta'_{4-ABNNR} = \begin{bmatrix} 0 & 0 & 0 & t & 0 & 0 & 0 & 0 \\ 0 & 0 & 0 & 0 & 0 & 0 & 0 & 0 \\ 0 & 0 & 0 & 0 & 0 & 0 & 0 & 0 \\ 0 & 0 & 0 & 0 & 0 & 0 & 0 & 0 \\ 0 & 0 & 0 & 0 & 0 & 0 & 0 & 0 \\ 0 & 0 & 0 & 0 & 0 & 0 & 0 & 0 \\ 0 & 0 & 0 & 0 & 0 & t & 0 & 0 \\ 0 & 0 & 0 & 0 & 0 & 0 & 0 & 0 \end{bmatrix} \quad (4)$$

For the formation of beta matrix of ZBNNRs, the interaction between the unit cell p and unit cell q of ZBNNRs is shown in the Eq. (5).

$$\beta_{4-ZBNNR} = \begin{bmatrix} 0 & t & 0 & 0 & 0 & 0 & 0 & 0 \\ 0 & 0 & 0 & 0 & 0 & 0 & 0 & 0 \\ 0 & 0 & 0 & 0 & 0 & 0 & 0 & 0 \\ 0 & 0 & t & 0 & 0 & 0 & 0 & 0 \\ 0 & 0 & 0 & 0 & 0 & t & 0 & 0 \\ 0 & 0 & 0 & 0 & 0 & 0 & 0 & 0 \\ 0 & 0 & 0 & 0 & 0 & 0 & 0 & 0 \\ 0 & 0 & 0 & 0 & 0 & 0 & t & 0 \end{bmatrix} \quad (5)$$

The relationship of the other side of the alpha matrix of ZBNNRs can be obtained by transposing the original beta matrix from Eq. (5) as shown in Eq. (6). The Eq. (6) represent the interaction between unit cell p and unit cell o.

Final Hamiltonian matrix for both ABNNRs and ZBNNRs can be formed by combining the alpha matrix and beta matrix into the Hamiltonian matrix. The 2D ABNNRs structure transformed into 1D structure when the ε substituted into the alpha matrix and t substituted into beta matrix. The electronic properties of ABNNRs and ZBNNRs can be studied and investigated by using the final Hamiltonian matrix.

$$\beta'_{4-ZBNNR} = \begin{bmatrix} 0 & 0 & 0 & 0 & 0 & 0 & 0 & 0 \\ t & 0 & 0 & 0 & 0 & 0 & 0 & 0 \\ 0 & 0 & 0 & t & 0 & 0 & 0 & 0 \\ 0 & 0 & 0 & 0 & 0 & 0 & 0 & 0 \\ 0 & 0 & 0 & 0 & 0 & 0 & 0 & 0 \\ 0 & 0 & 0 & 0 & t & 0 & 0 & 0 \\ 0 & 0 & 0 & 0 & 0 & 0 & 0 & t \\ 0 & 0 & 0 & 0 & 0 & 0 & 0 & 0 \end{bmatrix} \quad (6)$$

3.2.3 Hamiltonian operator

A general Hamiltonian matrix formed in Eq. (7) by using the alpha matrix, beta matrix and transposed beta matrix for the ABNNRs and ZBNNRs. The structure of a

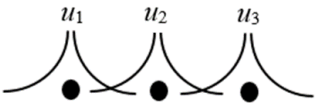

Fig. 6 Three hydrogen system, side-by-side with 1s wavefunction

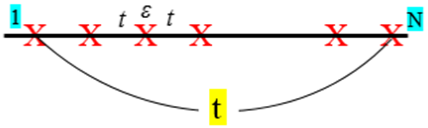

Fig. 7 A 1D N¬-atom chain with the arrow showing periodic boundary condition

Hamiltonian matrix determined by the length of ABNNRs and ZBNNRs structure.

$$H_{4-ABNNR\ or\ 4-ZBNNR,L=3} = \begin{bmatrix} \alpha_{11} & \beta_{12} & 0 \\ \beta_{21} & \alpha_{22} & \beta_{23} \\ 0 & \beta_{32} & \alpha_{33} \end{bmatrix} \quad (7)$$

From Eq. (7), the red colour highlighted alpha matrix represent the interaction of π-orbital within the unit cell. The blue colour highlighted beta matrix is the interaction between the unit cells. The other side of alpha matrix, which is the green colour highlighted beta matrix represent the transposed beta matrix from the original blue colour highlighted beta matrix. The final Hamiltonian matrix can be obtained by substituting the corresponding alpha matrix, beta matrix and transposed beta matrix of ABNNRs and ZBNNRs respectively into the general Hamiltonian matrix.

3.3 Calculation of band structure

The calculation of band structure is done by using the transport model and applying simplifying assumption followed by dispersion relation.

3.3.1 Transport models

A transport model is used to compute the electronic properties of BNNRs due to it involved a small device length which can be computed more accurately. The theory of transport model depends on the Schrödinger Eq., as shown in Eq. (8) (Schrödinger 1926). This Schrödinger Eq. preserved the wave-like properties of electrons due to its inherent wave function on the Eq. itself.

$$E\{\psi\} = [H]\{\psi\} \quad (8)$$

This Schrödinger Eq. is the basis functions for most of quantum transport models, including NEGF Formalism. This Schrödinger Eq. is used in this paper. The Hamiltonian operator, H, of the Schrödinger Eq. described the physical structure of the model. Once the Hamiltonian operator is defined, the available energy spectrums can be deduced when the Hamiltonian operator, H, is paired with the suitable wave function, ψ (Oxtoby *et al*. 2015).

3.3.2 Simplifying assumptions for device modelling

Numerical analysis of the Schrödinger Eq. is used for this work. The first simplifying assumption for the modelling devices is by using basis function only. Basis functions can be used to define a system. In the aspect of electronic properties, basis function can be used as a wavefunction of electrons in the molecules that involved in transport itself, unrelated to the rest of the valence band electrons. For instance, a 1D system consisting of three hydrogen atoms is considered, as shown in Fig. 6.

In Fig. 6, an electron is occupied on the outermost orbit of a hydrogen atom. This hydrogen 1*s* orbital is applied as the basis function to model the system. For a multilevel orbital system, such as a 2D boron nitride sheet is extended by using this concept. A 2D BN sheet has two shells, but, the π-electron of the $2p_z$ orbital and its respective wave function are considered as a basis function for this work. The wavefunction of 1*s* orbital overlaps with the adjacent hydrogen atom. Thus, the second simplifying assumption is made where the wavefunctions only affected by its nearest neighbour. This NNTB model is used for this simulation work.

A third simplifying assumption is the energy spectrum can be discretized into a matrix Eq.. This matrix Eq. can be used to solve the energy spectrum by using computational methods. This matrix Eq. is justified due to the structure of the lattice itself is made up of discrete atoms at the atomic level. With all the assumptions made and the Hamiltonian matrix constructed from Eq. (7), Eq. (9) is generated for the energy spectrum.

$$E\begin{Bmatrix}\psi_1\\ \psi_2\\ \psi_3\end{Bmatrix} = \begin{bmatrix} \alpha_{11} & \beta_{12} & 0 \\ \beta_{21} & \alpha_{22} & \beta_{23} \\ 0 & \beta_{32} & \alpha_{33} \end{bmatrix}\begin{Bmatrix}\psi_1\\ \psi_2\\ \psi_3\end{Bmatrix} \quad (9)$$

3.3.3 Dispersion relation

Dispersion relation of a system is defined as a function that energy of the electron and its wave vector are related. The dispersion relation is the relationship between the band energy, E and the wavenumber, k by applying the basis functions as the constraints. A range of k values is used to compute the band energy spectrum after the E-k relation is obtained successfully. The range of k values is selected to be within the first Brillouin zone, which corresponds to wavenumber $-\pi$ to π. Fig. 7 shows an N-atom 1D system to discuss the derivation of the dispersion relation.

The Hamiltonian matrix for N-atom chain can be constructed, as shown in Eq. (10). The ε represents the self-interaction energy of boron atom and nitrogen atom, and t represents the interaction energy between atoms.

$$E\begin{Bmatrix}\psi_1\\ \psi_2\\ \vdots\\ \psi_{N-1}\\ \psi_N\end{Bmatrix} = \begin{bmatrix} \varepsilon_B & t & 0 & \cdots & \cdots & t \\ t & \varepsilon_N & t & 0 & \ddots & \vdots \\ 0 & t & \varepsilon_B & t & 0 & \vdots \\ \vdots & \ddots & \ddots & \ddots & \ddots & \vdots \\ \vdots & \ddots & \ddots & \ddots & \ddots & \vdots \\ t & \cdots & \cdots & 0 & t & \varepsilon_N \end{bmatrix}\begin{Bmatrix}\psi_1\\ \psi_2\\ \vdots\\ \psi_{N-1}\\ \psi_N\end{Bmatrix} \quad (10)$$

The periodic boundary condition allows the whole matrix Eq. collapsed into a single linear Eq., as shown in Eq. (11).

$$E_{\psi_n} = +t_{\psi_{n-1}} + \varepsilon_{\psi_n} + t_{\psi_{n+1}} \quad (11)$$

The wavefunction can be approximated with a plane wave by transforming it into a function of wavenumber, k, as shown in Eq. (12).

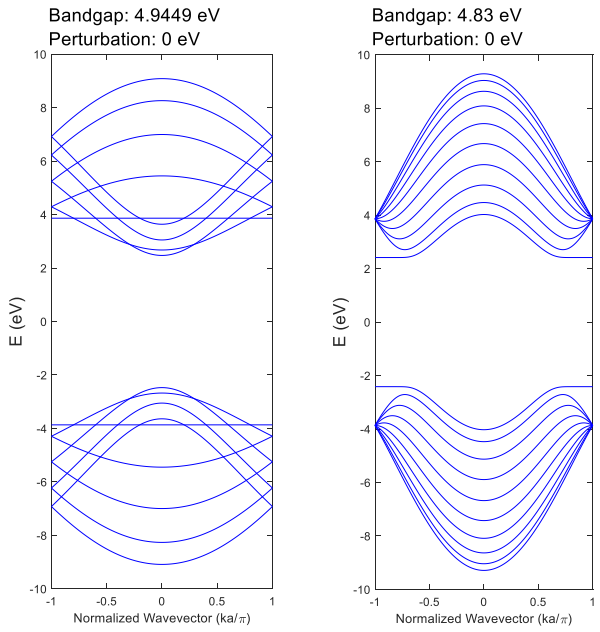

(a) (b)

Fig. 8 Band structure for nanoribbons without edge perturbation (a) 9-ABNNRs and (b) 10-ZBNNRs

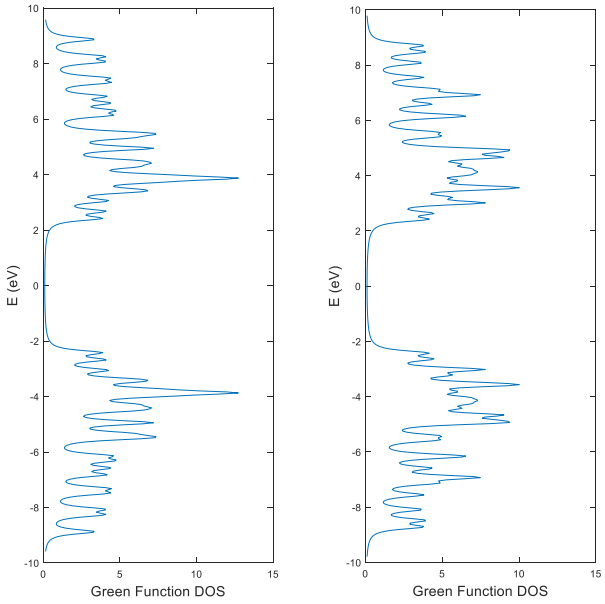

(a) (b)

Fig. 9 Green's Function DOS for nanoribbons without edge perturbation (a) 9-ABNNRs and (b) 10-ZBNNRs

$$\psi_n = \psi_0 e^{+inka} \tag{12}$$

Eq. (13) is obtained by dividing the *n*-th minus-one wave function with the *n*-th wave function.

$$\frac{\psi_{n-1}}{\psi_n} = \frac{e^{+i(n-1)ka}}{e^{+inka}} = e^{-ika} \tag{13}$$

Then, the Eq. (11) is transformed into Eq. (14) to obtain the final dispersion relation Equation.

$$E = te^{-ika} + \varepsilon + te^{+ika} \equiv \varepsilon + 2t\cos(ka) \tag{14}$$

Fig. 8 depicts the band structure for 9-ABNNRs 10-ZBNNRs without edge perturbation derived from Eq. (14).

3.4 Local DOS

Local DOS stated the number of states that occupied by a certain energy level interval in a unit cell. Local DOS can be simulated numerically by using delta function, δ. The Local DOS is computed by using Eq. (15).

$$\text{Local DOS(E)} = \sum_{i=1}^{N} \frac{1}{2\pi} \int \delta[E_i(k) - E]dk \tag{15}$$

The delta function, δ can be solved computationally by transformed it into Eq. (16) and substituted it into Eq. (15), then Eq. (17) is obtained.

$$\delta[E_i(k) - E] = \frac{\eta_G}{[E_i(k) - E]^2 + {\eta_G}^2} \tag{16}$$

$$\text{Local } DOS(E) = \sum_{i=1}^{N} \frac{1}{2\pi} \sum_{all\ k} \frac{\eta_G}{[E_i(k) - E]^2 + {\eta^2}_G} \tag{17}$$

The numerical method is used for the calculation of local DOS. The numerical method used did not consider the length of BNNRs. This is due to the calculation of local DOS use the information from the Hamiltonian matrix, including the eigenvalues of the Hamiltonian matrix for the computation of local DOS. The Hamiltonian matrix captured its full dimension for the computation and the simulation.

3.5 Green's function DOS

Green's Function DOS can be computed by using the Green's Function theory by using Eq. (18). G_F in the Eq. (18) indicated the retarded Green's Function, which is represented by Eq. (19). η in the Eq. (19) represented small imaginary value to prevent the inverse matrix from diverging, I is the identity matrix, and H is the Hamiltonian operator matrix.

$$Green's\ Function\ DOS = \frac{1}{\pi} Im[Trace[G_F] \tag{18}$$

$$G_F = [(E + i\eta) * I - H]^{-1} \tag{19}$$

The Green's Function DOS for 9-ABNNRs and 10-ZBNNRs, without edge perturbation, is depicted in Fig. 9, as derived from Eq. (19).

4. Armchair boron nitride nanoribbons (ABNNRs)

4.1 Introduction

The energy band structure contains a lot of information regarding the ABNNRs. The classification of electronic properties can be obtained from the band structure, bandgap value, local DOS, and Green's Function DOS. The material properties can be classified into metal, semiconductor, and insulator. The edge perturbation applied on the top-edge atoms and bottom-edge atoms of ABNNRs for a range of -1

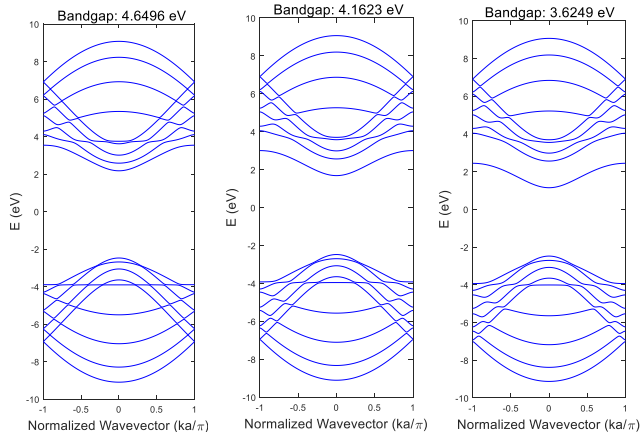

Fig. 10 Band structure after edge perturbation of (a) -1 eV, (b) -2 eV, and (c) -3 eV on top-edge boron atoms of 9-ABNNRs

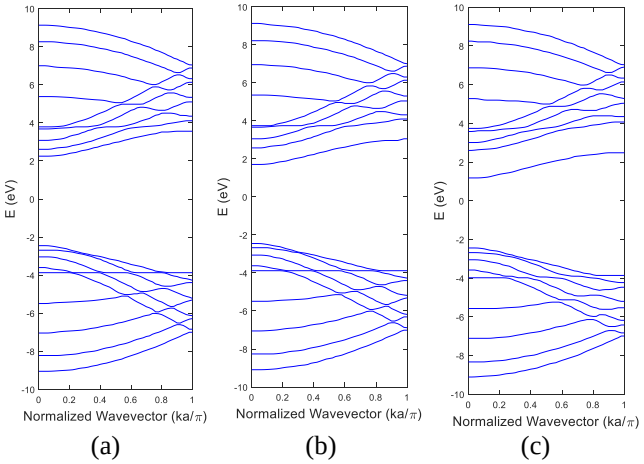

Fig. 11 Band structure after edge perturbation of (a) -1 eV, (b) -2 eV, and (c) -3 eV on top-edge boron atoms of 9-ABNNRs from benchmark reference work (DiBenedetto 2017)

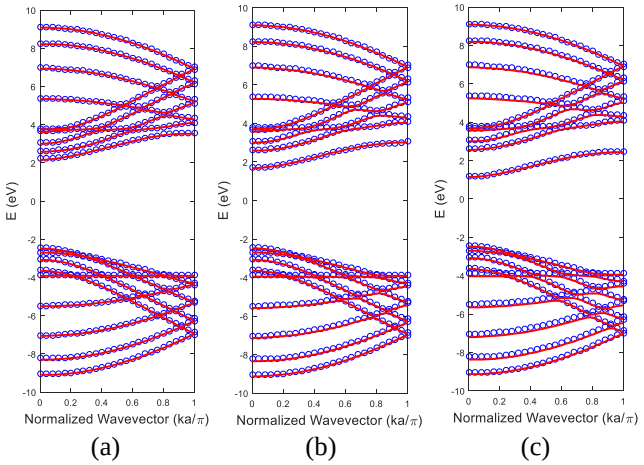

Fig. 12 Comparison result of band structure after edge perturbation applied of (a) -1, (b) -2, and (c) -3 eV on top-edge boron atoms of 9-ABNNRs. Blue circles indicated result from benchmark reference work (DiBenedetto 2017). Red lines indicated result from this work

eV until -3 eV from the original onsite energy of boron atom (ε_B = -6.64 eV) and nitrogen atom (ε_N = -11.47 eV). The onsite energy changes can cause high localized atom at the edge of BNNRs (Aliofkhazraei *et al*. 2016). The calculations are energy plots versus the wave vector. The *k*-space in the graph acted as a wave vector, where *k* represented the momentum state due to the structure of the material. The local DOS can be obtained from the eigenvalues from the band structure. Local DOS is the number of states occupied by electrons at a certain energy level by a unit cell. Green's Function DOS is the total number of states occupied by electrons which considered the length of ABNNRs.

4.2 Band structure

Fig. 2 shows the edge structure of 9-ABNNRs with length is 3. The edge perturbation effect applied on the top-edge boron atom with the range of -3 eV until +3 eV from the original onsite energy of boron atom (ε_B = -6.64 eV). Fig. 10 shows the band structure when the perturbation strength from -1 eV until -3 eV applied on the top-edge boron atom for 9-ABNNRs with length is 3.

Fig. 11 shows the band structure when the perturbation strength from -1 eV until -3 eV applied on the top-edge boron atom for 9-ABNNRs with length is 3 from benchmark reference work.

In Fig. 10, the conduction bands experienced distortion, and the first conduction band pulled down toward the Fermi energy level when edge perturbation increased. The valence bands experienced distortion too. This phenomenon happened due to the top-edge boron atom perturbed with negative edge perturbation strength. Hence the eigenvalues of the Hamiltonian changed. The bandgap energy decreased from 4.6496 eV until 3.6249 eV when negative edge perturbation strength increased. This phenomenon happened because the top-edge boron atoms became more negative when negative edge perturbation strength increased. Thus, the bandgap decreased due to the shifting of the first conduction band when negative edge perturbation increased. In Fig. 11, the whole conduction bands and valence bands experienced distortion too. The first conduction band pulled down toward the Fermi energy level when negative edge perturbation increased. The band structure in Fig. 11 shows similar to the band structure in Fig. 10 after the wavenumber, *k*=0.

The comparison results are made between this simulation work and the benchmark reference work. The red line represents this simulation work, whereas the blue line represents the benchmark reference work (DiBenedetto 2017). Both graphs digitized first by using GetData Graph Digitizer software and then plotted together by using Matlab software. Fig. 12 shows the comparison result of band structure after edge perturbation applied on the top-edge boron atoms of 9-ABNNRs.

The shape of the band strucre between this simulation work and the benchmark reference work similar and fit together. However, the range of *x*-value is chosen to normalize to 1 due to this simulation work considered the whole system is periodic, where the values of wavenumber,

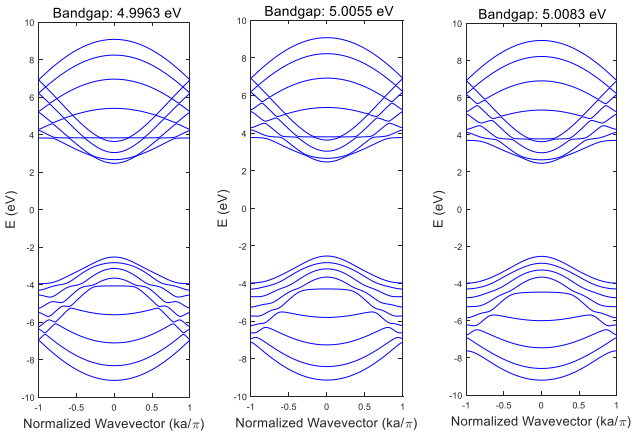

Fig. 13 Band structure after edge perturbation of (a) -1 eV, (b) -2 eV, and (c) -3 eV on top-edge nitrogen atoms of 9-ABNNRs

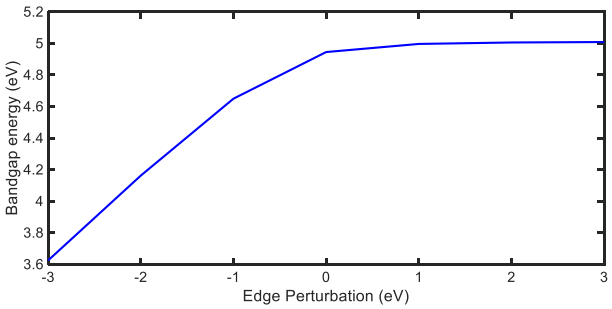

Fig. 14 Bandgap energy when edge perturbation applied on the top-edge boron atoms of 9-ABNNRs

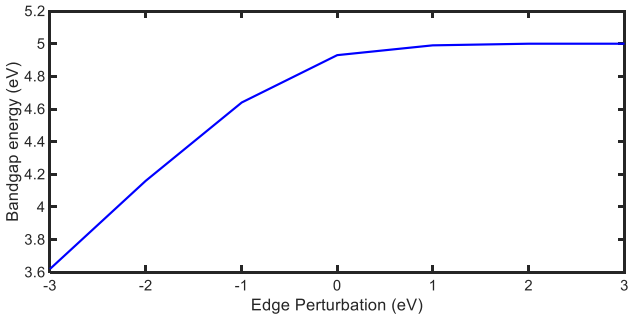

Fig. 15 Bandgap energy when edge perturbation applied on the top-edge boron atoms in 9-ABNNRs with selected edge atoms circled in green from benchmark reference work (DiBenedetto 2017)

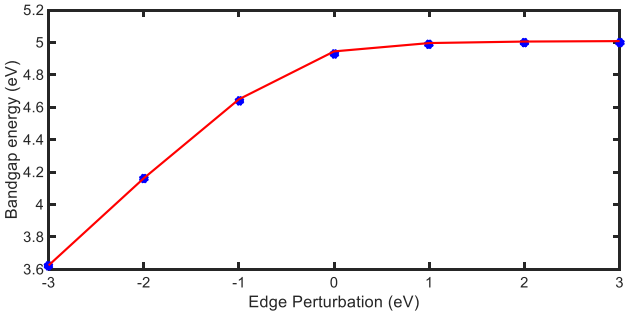

Fig. 16 Comparison result of bandgap energy after edge perturbation applied of -3 eV until 3 eV on top-edge boron atoms of 9-ABNNRs. Blue dot indicated result from benchmark reference work (DiBenedetto 2017). Red line indicated result from this simulation work

k is within the first Brillouin zone to represent the whole system which corresponds to the wavenumber of $-\pi$ to π (Goh *et al*. 2018). For the benchmark reference work, the periodic boundary condition is considered. It is a range of boundary conditions chosen for approximating a large system by using a small part called a unit cell. This unit cell from a large system can produce the needed information (Makov and Payne 1995). The edge perturbation effect is applied on the top-edge nitrogen atoms with the range of -1 eV until -3 eV from the original onsite energy of nitrogen atoms (ε_N = -11.47 eV).

Fig. 13 shows the band structure after edge perturbation strength of -1 eV until -3 eV applied on the top-edge nitrogen atoms of 9-ABNNRs. In Fig. 13, the conduction bands and valence bands experienced less distortion when negative edge perturbation strength applied on the top-edge nitrogen atoms.

4.3 Bandgap energy

The edge perturbation is applied on the top-edge boron atoms of 9-ABNNRs. Fig. 14 shows the bandgap energy graph when edge perturbation strength from -3 eV until +3 eV applied on the top-edge boron atoms for 9-ABNNRs. Fig. 15 shows the bandgap energy after edge perturbation from the benchmark reference work. In Fig. 14, the bandgap energy increased from roughly 3.6 eV until around 4.65 eV when edge perturbation of -3 eV, -2 eV, and -1 eV applied on the top-edge boron atoms respectively. However, when edge perturbation of +1 eV, +2 eV, and +3 eV is applied on the top-edge boron atoms, the bandgap energy remained constant at almost 5.0 eV. This phenomenon happened due to more positively of top-edge boron atoms that did not affect the shifting of the conduction band. Thus, the bandgap remained constant. In Fig. 13, the bandgap energy shows a similar result with the bandgap energy from Fig. 14. Fig. 16 shows the comparison result of bandgap energy after edge perturbation applied on 9-ABNNRs.

In Fig. 16, the shape of bandgap energy for this simulation work and the benchmark reference work is similar. The bandgap energy values for this simulation work fulfilled the bandgap energy values from the benchmark reference work for each edge perturbation strength applied on the top-edge boron atoms of the 9-ABNNRs. Next, the bandgap energy is shown for edge perturbation applied on the top-edge nitrogen atoms of 9-ABNNRs. The result of the bandgap energy from this simulation work is compared with the benchmark reference work.

Fig. 17 shows the bandgap energy graph when edge perturbation strength from -3 eV until +3 eV applied on the top-edge nitrogen atoms for 9-ABNNRs. In Fig. 17, the bandgap energy decreased from 4.6 eV until 3.6 eV when positive edge perturbation applied on the top-edge nitrogen atoms of 9-ABNNRs. This phenomenon is happened due to shifting of the top valence band to the Fermi energy level at

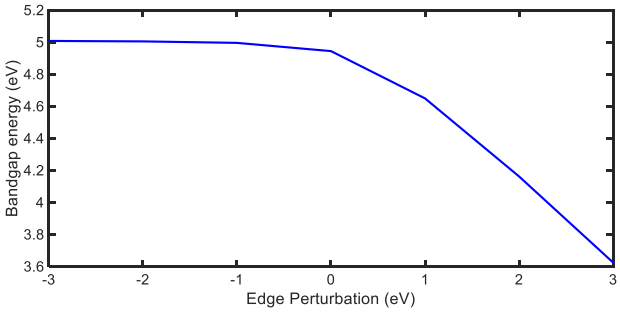

Fig. 17 Bandgap energy when edge perturbation applied on the top-edge nitrogen atoms of 9-ABNNRs

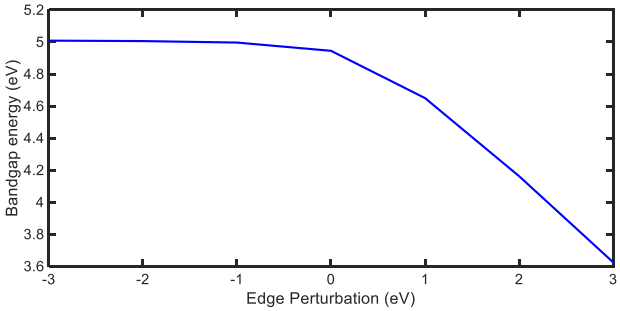

Fig. 18 Bandgap energy when edge perturbation applied on the top-edge nitrogen atoms in 9-ABNNRs from benchmark reference work (DiBenedetto 2017)

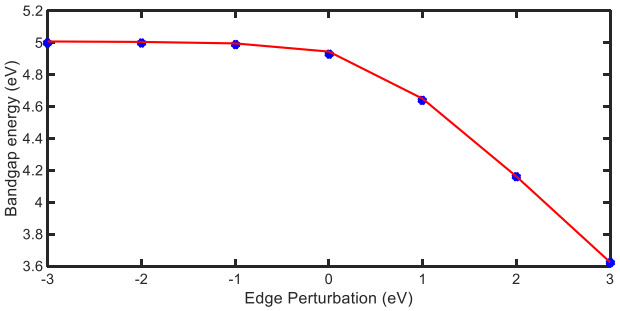

Fig. 19 Comparison result of bandgap energy after edge perturbation applied of -3 eV until 3 eV on top-edge nitrogen atoms of 9-ABNNRs. Blue dot indicated result from benchmark reference work (DiBenedetto 2017). Red line indicated result from this simulation work.

k=0 and caused bandgap decreasing. However, the bandgap energy remained nearly constant at 5 eV when negative edge perturbation strength applied. In Fig. 18, the overall shape of the bandgap energy graph shows similar to the bandgap energy graph in Fig. 17.

The comparison result is made between this simulation work, and benchmark reference work is shown in Fig. 19. The bandgap energy graph from this simulation work and benchmark reference work shows similar and fit together, as shown in Fig. 19. The bandgap energy for every distinct edge perturbation strength is similar for this simulation work and benchmark reference work.

4.4 Local DOS

Fig. 20 shows the local DOS when the edge perturbation

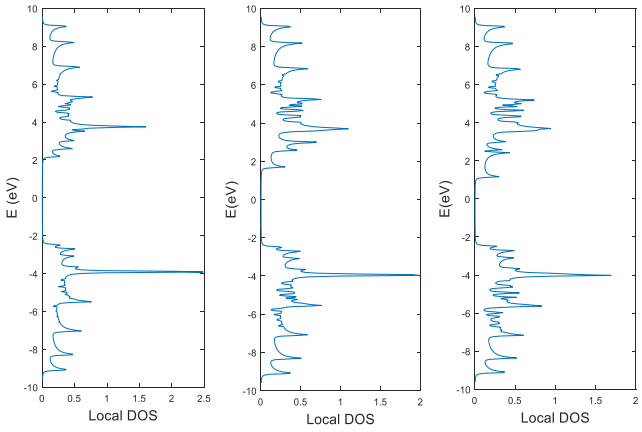

(a) (b) (c)

Fig. 20 Local DOS after edge perturbation of (a) -1 eV, (b) -2 eV, and (c) -3 eV on top-edge boron atoms of 9-ABNNRs

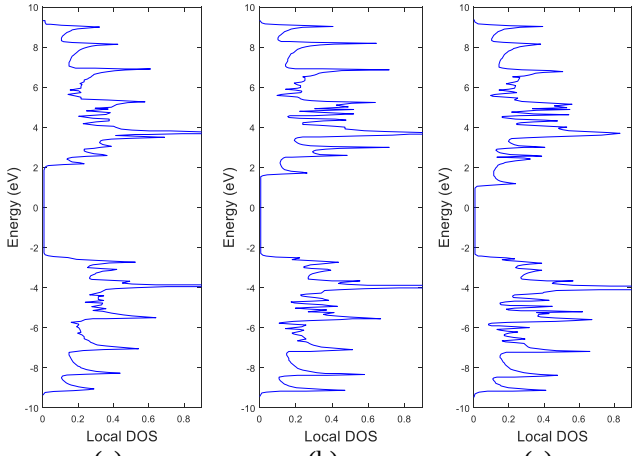

(a) (b) (c)

Fig. 21 Local DOS after edge perturbation of (a) -1 eV, (b) -2 eV, and (c) -3 eV on top-edge boron atoms of 9-ABNNRs from benchmark reference work (DiBenedetto 2017)

strength from -1 eV until -3 eV applied on the top-edge boron atom for 9-ABNNRs. Fig. 19 shows the local DOS after edge perturbation of -1 eV until -3 eV applied on 9-ABNNRs from benchmark reference work. In Fig. 20, the local DOS disrupted for conduction band lower than 7 eV from each continuous curves when negative edge perturbation strength increased. This phenomenon happened due to the eigenvalues of the Hamiltonian matrix changed after edge perturbation. The most obvious change is the curve at 5 eV moved more vigorously when edge perturbation strength increased. The valence band experienced distortion as well.

In Fig. 21, the local DOS disrupted for conduction bands and valence bands too. The curve at 4 eV moved more vigorously when edge perturbation strength increased. Fig. 22 illustrates the comparative outcomes of the local DOS following edge perturbation on 9-ABNNRs. While the local DOS profiles from both this study and the benchmark reference exhibit analogous shapes, the peaks within the continuous curves vary. This peak variation stems from the

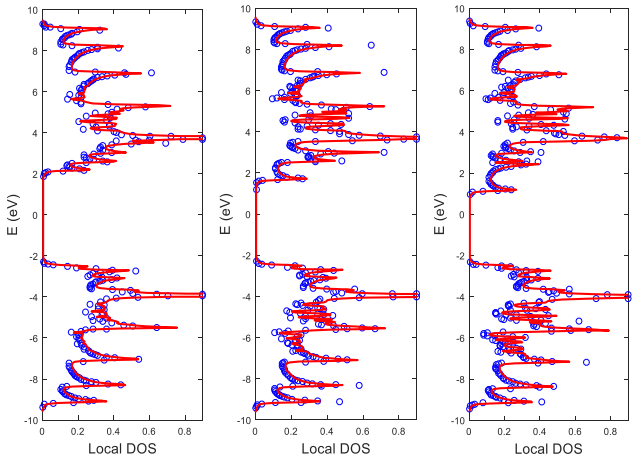

(a) (b) (c)

Fig. 22 Comparison result of local DOS after edge perturbation applied of (a) -1 eV, (b) -2 eV, and (c) -3 eV ontop-edge boron atoms of 9-ABNNRs. Blue line indicated result from benchmark reference work (DiBenedetto 2017). Red line indicated result from this simulation work

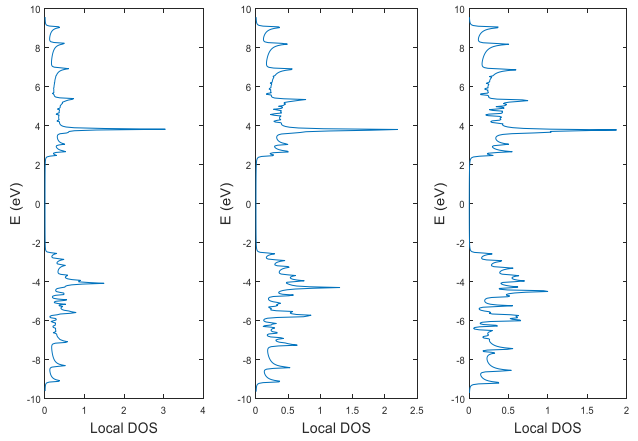

(a) (b) (c)

Fig. 23 Local DOS after edge perturbation of (a) -1 eV, (b) -2 eV, and (c) -3 eV on top-edge nitrogen atoms of 9-ABNNRs

local DOS computation through band structure in our simulation. Our system is characterized by the first Brillouin zone, and a numerical approach was employed. Notably, our numerical method did not account for the system's entire length. Conversely, the benchmark reference computed the local DOS using a semi-analytical technique, incorporating the summation of all sites, inclusive of the imaginary components of both the retarded and advanced Green's Functions (DiBenedetto 2017).

Subsequently, edge perturbation was administered to the top-edge nitrogen atoms of 9-ABNNRs. Fig. 23 depicts the local DOS as the edge perturbation strength ranges from -1 eV to -3 eV on these atoms. As observed in Fig. 23, the conduction and valence bands exhibit reduced delocalization when a negative edge perturbation strength is applied to the top-edge nitrogen atoms.

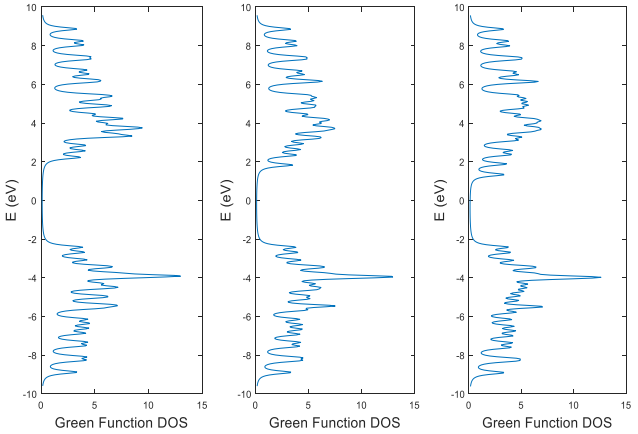

(a) (b) (c)

Fig. 24 Green's Function DOS after edge perturbation of (a) -1 eV, (b) -2 eV, and (c) -3 eV on top-edge boron atoms of 9-ABNNRs

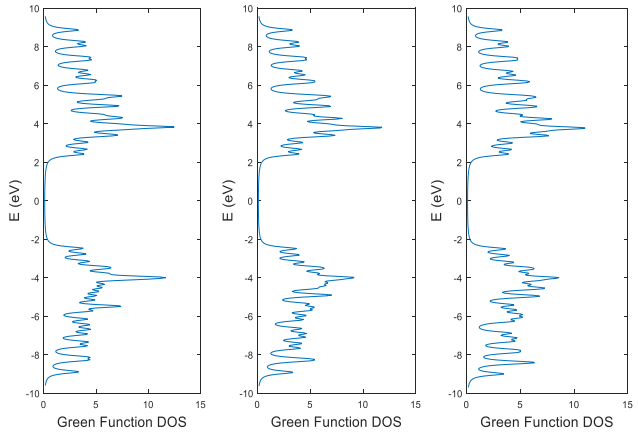

(a) (b) (c)

Fig. 25 Green's Function DOS after edge perturbation of (a) -1 eV, (b) -2 eV, and (c) -3 eV on top-edge nitrogen atoms of 9-ABNNRs

4.5 Green's Function DOS

Green's Function DOS reveals the total number of states that occupied by the electrons at a particular energy level, with the information of the length of BNNRs. Fig. 24 shows Green's Function DOS when the edge perturbation strength from -1 eV until -3 eV applied on the top-edge boron atoms for 9-ABNNRs. In Fig. 24, the conduction bands experienced distortion and pulled towards the Fermi energy level. The Green's Function DOS at 5 eV energy level and below experienced significant distortion when negative edge perturbation strength increasing. The valence bands at -5 eV and above experienced distortion too. This distortion due to edge perturbation can be reverted as the band structure shown in Fig. 10 and local DOS shown in Fig. 20. The edge perturbation is then applied on the top-edge nitrogen atoms of 9-ABNNRs.

Fig. 25 shows Green's Function DOS when the edge perturbation strength from -1 eV until -3 eV applied on the top-edge boron atoms for 9-ABNNRs. In Fig. 25, when

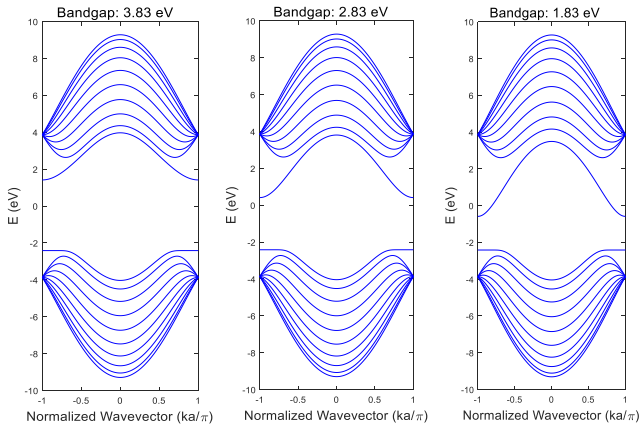

Fig. 26 Band structure after edge perturbation strength of (a) -1 eV, (b) -2 eV, and (c) -3 eV applied on top-edgeboron atoms of 10-ZBNNRs

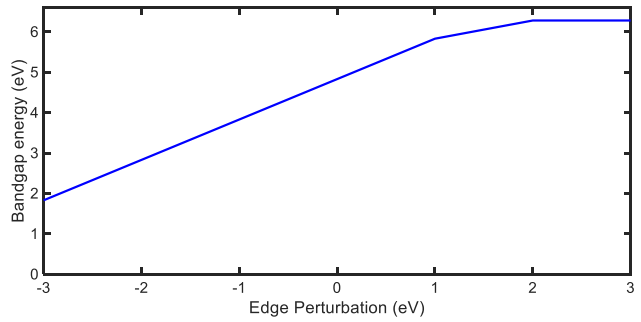

Fig. 27 Bandgap energy when edge perturbation applied on the top-edge boron atoms of 10-ZBNNRs

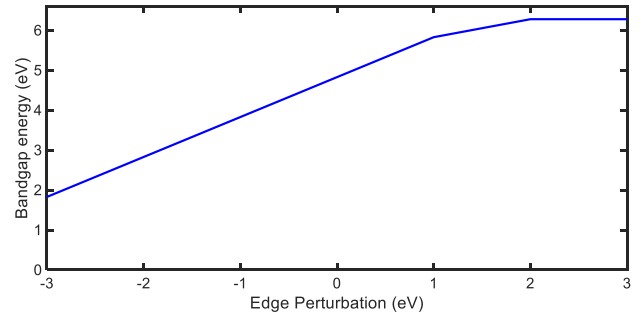

Fig. 28 Bandgap energy values when edge perturbation applied to top-edge boron atoms for 10-ZBNNRs from benchmark reference work (DiBenedetto 2017)

negative edge perturbation applied on the top-edge nitrogen atoms, the conduction bands and valence bands experienced less distortion. The edge perturbation strengths from -1 eV until -3 eV are applied on the top-edge boron atoms and top-edge nitrogen atoms of 9-ABNNRs, respectively. The simulation result included band structure, bandgap energy, local DOS, and Green's Function DOS. Then, the simulation result from this simulation work and benchmark reference work are compared and analysed on the top-edge boron atoms.

From the comparison results, the band structure and bandgap energy for edge perturbation strength from -1 eV until -3 eV applied on the top-edge boron atoms show similar and fitted together. However, the comparison result for local DOS shows similar but different in peak for continuous curves. This phenomenon happened due to the numerical method is used for this simulation work, and the semi-analytical method is used for the benchmark reference work. From the simulation result, the band structure, bandgap energy, local DOS, and Green's Function DOS of top-edge atoms after edge perturbation, are found that to be the same as the bottom-edge atoms after edge perturbation. This similarity is due to the configuration of the top-edge, and bottom-edge of 9-ABNNRs is a symmetrical structure. Thus, they have similar electronic properties after edge perturbation.

5. Zigzag Boron Nitride Nanoribbons (ZBNNRs)

5.1 Introduction

A ZBNNRs with width, N=10, and length, L=3 considered for the simulation of the band structure, band gap energy value, local DOS, and Green's Function DOS. The edge perturbation strength from -1 eV until -3 eV selected to be applied on the top-edge boron atoms of the 10-ZBNNRs. This range of edge perturbation strength adjusted on the original onsite energy of the boron atoms (ε_B = -6.64 eV).

5.2 Band structure

Fig. 26 shows the band structure when the edge perturbation strength from -1 eV until -3 eV applied on the top-edge boron atoms for 10-ZBNNRs. In Fig. 26, the first conduction band distorted and pulled towards the Fermi energy level when negative edge perturbation applied increasing from -1 eV until -3 eV.

5.3 Bandgap energy

The edge perturbation is applied on the top-edge boron atoms of 10-ZBNNRs. Fig. 27 shows the bandgap energy graph when edge perturbation strength from -3 eV until +3 eV applied on the bottom-edge nitrogen atoms for 10-ZBNNRs. Fig. 28 shows the bandgap energy when edge perturbation applied on top-edge nitrogen atoms for 10-ZBNNRs from benchmark reference work. In Fig. 27, the bandgap energy at edge perturbation of +1 eV is roughly at 3.8 eV and decreased until roughly at 1.8 eV when +3 eV edge perturbation applied on the top-edge boron atoms of 10-ZBNNRs. The decreasing of bandgap energy is occurred due to the shifting of the first conduction band towards the Fermi energy level. When negative edge perturbation applied, the bandgap energy shows no significant effect on it. The benchmark reference work from Fig. 28 shows a similar bandgap energy graph with Fig. 27. Fig. 29 shows the comparison result for the bandgap energy when edge perturbation applied on the top-edge boron atoms. In Fig. 29, the comparison result between this simulation work and the benchmark reference work is similar and fitted together when edge perturbation applied on the top-edge boron atoms. The red line in Fig. 29 represents the outcomes of this simulation, which focused on the top-edge boron atoms.

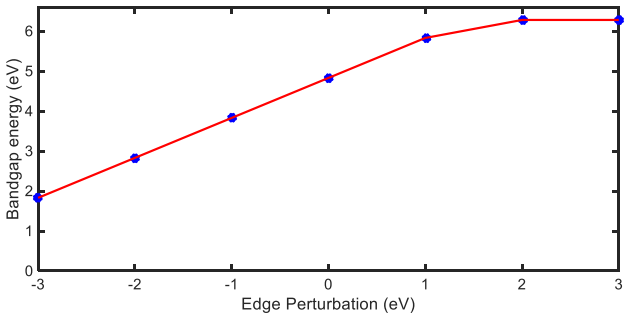

Fig. 29 Comparison result of bandgap energy after edge perturbation of -3 eV until +3 eV applied on top-edge boron atoms of 10-ZBNNRs. Blue dot indicated result from benchmark reference work (DiBenedetto 2017).

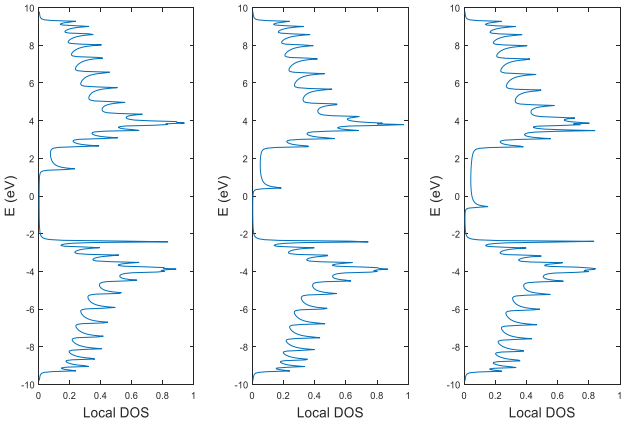

(a) (b) (c)

Fig. 30 Local DOS after edge perturbation of (a) -1 eV, (b) -2 eV, and (c) -3 eV applied on top-edge boron atoms of 10-ZBNNRs

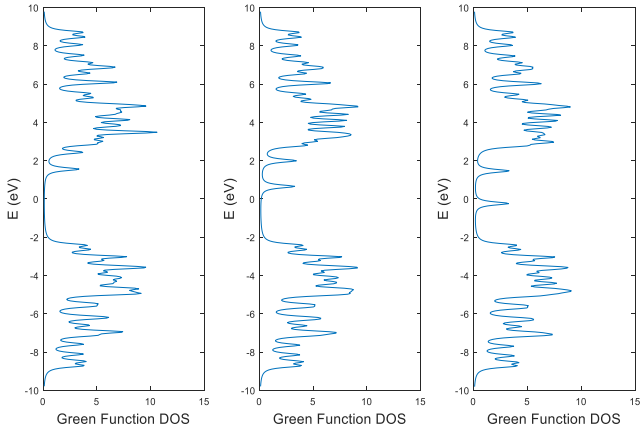

(a) (b) (c)

Fig. 31 Green's Function DOS after edge perturbation of (a) -1 eV, (b) -2 eV, and (c) -3 eV applied on top-edge boron atoms of 10-ZBNNRs

It reveals that the bandgap energy remains consistent, across the range of edge perturbations from -3 eV to +3 eV.

5.4 Local DOS

Fig. 30 shows the local DOS when the edge perturbation strength from -1 eV until -3 eV applied on the top-edge boron atoms for 10-ZBNNRs. The conduction bands of local DOS in Fig. 30 experienced high distortion, and the bandgap energy is reduced. The valence bands did not experience any distortion. This phenomenon happened due to the top-edge of 10-ZBNNRs consist of boron atom only.

5.5 Green's Function DOS

Fig. 31 shows the Green's Function DOS when the edge perturbation strength from -1 eV until -3 eV applied on the top-edge boron atoms for 10-ZBNNRs. The conduction bands in Fig. 31 pulled towards the Fermi energy level and causing bandgap energy to decrease. The distortion of conduction bands can be reflected as the band structure shown in Fig. 26 and local DOS in Fig. 30.

6. Conclusions

In this study and the benchmark reference work, a tight-binding parameter of -3.01834 eV was employed. In particular, varying this parameter in electronic property simulations could lead to different outcomes, as changes in the tight-binding parameters alter the Hamiltonian matrix. While our study utilized a numerical method, making assumptions to represent the entire system and being length-independent for both ABNNRs and ZBNNRs, the benchmark reference employed a semi-analytical approach. This latter method, though comprehensive, is computationally intensive and time-consuming. When comparing our results with the benchmark, we found that the band structure and bandgap energy graphs for the top-edge boron atoms of ABNNRs aligned closely. However, while the local DOS graphs for these atoms were similar, there were noticeable differences in the peak values of the continuous curves. Furthermore, a significant addition we made in our script is the inclusion of input parameters for both the width and length of the unit cell. This enhancement allows for greater flexibility and adaptability, making our simulation applicable to various dimensions of BNNRs. Another noteworthy aspect of our research is the presentation of two types of DOS calculations: one based on numerical methods and the other derived from Green's Function. This dual approach provides a comprehensive view of the electronic properties and offers a more in-depth analysis of BNNRs. This feature not only broadens the scope of our research but also provides a tool for researchers to explore a wider range of BNNR configurations and electronic behaviours.

Acknowledgments

The authors express gratitude for the financial support provided by UTM Fundamental Research, UTMFR (Cost Centre No.: Q.J130000.3823.22H76), which facilitated the seamless progression of thi research. Michael Tan extends his appreciation to the UTM Research Management Centre (RMC) for fostering a conducive environment, enabling his results-driven team to produce industry-standard outcomes.

References

Aliofkhazraei, M., Ali, N., Milne, W.I., Ozkan, C.S., Mitura, S. and Gervasoni, J.L. (2016), *Graphene Science Handbook: Nanostructure and Atomic Arrangement*, CRC Press.

Attaccalite, C., Bockstedte, M., Marini, A., Rubio, A. and Wirtz, L. (2011), "Coupling of excitons and defect states in boron-nitride nanostructures", *Phys. Rev. B*, **83**(14), 144115. https://doi.org/10.1103/PhysRevB.83.144115.

Baggott, J. (2000), *The meaning of quantum theory: a guide for students of chemistry and physics*, Oxford Science Publications

Chegel, R. (2016), "Engineering the electronic structure and band gap of boron nitride nanoribbon via external electric field", *Appl. Phys. A*, **122**(6), 567. https://doi.org/10.1007/s00339-016-0095-7.

Chuan, M.W., Lok, S.Z., Hamzah, A., Alias, N.E., Sultan, S.M., Lim, C.S. and Tan, M.L.P. (2023), "Electronic properties of graphene nanoribbons with Stone-Wales defects using the tight-binding method", *Adv. Nano Res.*, **14**(1), 1-15. https://doi.org/10.12989/anr.2023.14.1.001.

Chuan, M.W., Wong, K.L., Hamzah, A., Rusli, S., Alias, N.E., Lim, C.S. and Tan, M.L.P. (2020a), "2D honeycomb silicon: a review on theoretical advances for silicene field-effect transistors", *Curr. Nanosci.*, **16**(4), 595-607. https://doi.org/10.2174/1573413715666190709120019.

Chuan, M.W., Wong, K.L., Hamzah, A., Rusli, S., Alias, N.E., Lim, C.S. and Tan, M.L.P. (2020b), "A review of the top of the barrier nanotransistor models for semiconductor nanomaterials", *Superlatt. Microstruct.*, **140**, 17. https://doi.org/10.1016/j.spmi.2020.106429.

Chuan, M.W., Wong, Y.B., Hamzah, A., Alias, N.E., Sultan, S.M., Lim, C.S. and Tan, M.L.P. (2022), "Electronic properties of monolayer silicon carbide nanoribbons using tight-binding approach", *Adv. Nano Res.*, **12**(2), 213-221. https://doi.org/10.12989/anr.2022.12.2.213.

Datta, S. (2005), *Quantum Transport: Atom to Transistor*, Cambridge University Press, Cambridge. https://doi.org/10.1017/CBO9781139164313.

DiBenedetto, A. (2017), *The Electronic Properties of Hexagonal Boron Nitride and Graphene Nanoribbons*, Ball State University.

DiBenedetto, A. and Khatun, M. (2018), "Electronic properties of edge-terminated zigzag hexagonal boron nitride nanoribbons", *J. Phys. D Appl. Phys.*, **52**(2), 025301. https://doi.org/10.1088/1361-6463/aae674.

Du, A.J., Smith, S.C. and Lu, G.Q. (2007), "First-principle studies of electronic structure and C-doping effect in boron nitride nanoribbon", *Chem. Phys. Lett.*, **447**(4), 181-186. https://doi.org/10.1016/j.cplett.2007.09.038.

Goh, E., Chin, H., Wong, K., Indra, I. and Tan, M. (2018), "Modeling and simulation of the electronic properties in graphene nanoribbons of varying widths and lengths using tight-binding Hamiltonian", *J. Nanoelectr. Optoelectr.*, **13**, 289-300. https://doi.org/10.1166/jno.2018.2206.

Goringe, C.M., Bowler, D.R. and Hernández, E. (1997), "Tight-binding modelling of materials", *Reports Prog. Phys.*, **60**(12), 1447-1512. https://doi.org/10.1088/0034-4885/60/12/001.

Guerra, T., Araújo, L.R.S. and Azevedo, S. (2019), "Magnetic and electronic properties of diamond-shaped graphene-boron nitride nanoribbons and nanoflakes", *J. Phys. Chem. Solids*, **135**, 109085. https://doi.org/10.1016/j.jpcs.2019.109085.

Huang, B., Lee, H., Gu, B.L., Liu, F. and Duan, W. (2012), "Edge stability of boron nitride nanoribbons and its application in designing hybrid BNC structures", *Nano Res.*, **5**(1), 62-72. https://doi.org/10.1007/s12274-011-0185-y.

Izyumskaya, N., Demchenko, D.O., Das, S., Özgür, Ü., Avrutin, V. and Morkoç, H. (2017), "Recent development of boron nitride towards electronic applications", *Adv. Electr. Mater.*, **3**(5), 1600485. https://doi.org/10.1002/aelm.201600485.

Jin, L., Li-Zhong, S. and Jian-Xin, Z. (2010), "Strain effects on electronic properties of boron nitride nanoribbons", *Chinese Phys. Lett.*, **27**(7), 077101. https://doi.org/10.1088/0256-307X/27/7/077101.

Kumar, C.V. and Pattammattel, A. (2017), *Chapter 1 - Discovery of graphene and beyond*, Elsevier.

Lee, S.H. and Jhi, S.H. (2015), "A first-principles study on three-dimensional covalently-bonded hexagonal boron nitride nanoribbons", *J. Phys. Condens. Matter.*, **27**(7), 075301. https://doi.org/10.1088/0953-8984/27/7/075301.

Lim, W.H., Hamzah, A., Ahmadi, M.T. and Ismail, R. (2017). "Analytical study of the electronic properties of boron nitride nanosheet", *2017 IEEE Regional Symposium on Micro and Nanoelectronics (RSM)*, 23-25 August.

Lopez-Bezanilla, A., Huang, J., Terrones, H. and Sumpter, B.G. (2012), "Structure and electronic properties of edge-functionalized armchair boron nitride nanoribbons", *J. Phys. Chem. C*, **116**(29), 15675-15681. https://doi.org/10.1021/jp3036583.

Ma, H., Lin, S.H., Carpenter, R.W., Rice, P. and Sankey, O.F. (1993), "Ab initio calculation of band structure, x-ray emission, quantum yield, and electron-energy-loss spectra of hexagonal boron nitride", *J. Appl. Phys.*, **73**(11), 7422-7426. https://doi.org/10.1063/1.353983.

Makov, G. and Payne, M.C. (1995), "Periodic boundary conditions in ab initio calculations", *Phys. Rev. B*, **51**(7), 4014-4022. https://doi.org/10.1103/PhysRevB.51.4014.

Morrell, R. (2000), *4.01 - Matrix Materials*, Pergamon, Oxford.

Oxtoby, D., Gillis, H. and Butler, L. (2015), *Principles of modern chemistry*. *Cengage Learning*, Saunders College Publishing, Fort Worth, Texas, U.S.A.

Park, C.H. and Louie, S.G. (2008), "Energy gaps and stark effect in boron nitride nanoribbons", *Nano Lett.*, **8**(8), 2200-2203. https://doi.org/10.1021/nl080695i.

Ribeiro, R.M. and Peres, N.M.R. (2011), "Stability of boron nitride bilayers: Ground-state energies, interlayer distances, and tight-binding description", *Phys. Rev. B*, **83**(23), 235312. https://doi.org/10.1103/PhysRevB.83.235312.

Schrödinger, E. (1926), "An Undulatory Theory of the Mechanics of Atoms and Molecules", *Phys. Rev.*, **28**(6), 1049-1070. https://doi.org/10.1103/PhysRev.28.1049.

Song, L., Ci, L., Lu, H., Sorokin, P.B., Jin, C., Ni, J., Kvashnin, A.G., Kvashnin, D.G., Lou, J., Yakobson, B.I. and Ajayan, P.M. (2010), "Large scale growth and characterization of atomic hexagonal boron nitride layers", *Nano Lett.*, **10**(8), 3209-3215. https://doi.org/10.1021/nl1022139.

Sutton, A.P., Finnis, M.W., Pettifor, D.G. and Ohta, Y. (1988), "The tight-binding bond model", *J. Phys. C Solid State Phys.*, **21**(1), 35-66. https://doi.org/10.1088/0022-3719/21/1/007.

Tang, S. and Cao, Z. (2010), "Carbon-doped zigzag boron nitride nanoribbons with widely tunable electronic and magnetic properties: insight from density functional calculations", *Phys. Chem. Chem. Phys.*, **12**(10), 2313-2320. https://doi.org/10.1039/B920754F.

Watanabe, K., Taniguchi, T. and Kanda, H. (2004), "Direct-bandgap properties and evidence for ultraviolet lasing of hexagonal boron nitride single crystal", *Nature Mater.*, **3**(6), 404-409. https://doi.org/10.1038/nmat1134.

Xie, Z.X., Tang, L.M., Pan, C.N., Chen, Q. and Chen, K.Q. (2013), "Ballistic thermoelectric properties in boron nitride nanoribbons", *J. Appl. Phys.*, **114**(14), 144311. https://doi.org/10.1063/1.4824750.

Zeng, H., Zhi, C., Zhang, Z., Wei, X., Wang, X., Guo, W., Bando, Y. and Golberg, D. (2010), "White graphenes": boron nitride nanoribbons via boron nitride nanotube unwrapping", *Nano Lett.*, **10**(12), 5049-5055.

Zhao, K., Zhao, M., Wang, Z. and Fan, Y. (2010), "Tight-binding model for the electronic structures of SiC and BN nanoribbons", *Physica E*, **43**(1), 440-445. https://doi.org/10.1016/j.physe.2010.08.025.

Zheng, F., Sasaki, K.I., Saito, R., Duan, W. and Gu, B.L. (2009), "Edge states of zigzag boron nitride nanoribbons", *J. Phys. Soc. Japan*, **78**(7), 074713. https://doi.org/10.1143/JPSJ.78.074713.

Zheng, F., Zhou, G., Liu, Z., Wu, J., Duan, W., Gu, B.L. and Zhang, S.B. (2008), "Half metallicity along the edge of zigzag boron nitride nanoribbons", *Phys. Rev. B*, **78**(20), 205415. https://doi.org/10.1103/PhysRevB.78.205415.

Zunger, A. (1974), "A molecular calculation of electronic properties of layered crystals. I. Truncated crystal approach for hexagonal boron nitride", *J. Phys. C Solid State Phys.*, **7**(1), 76-95. https://doi.org/10.1088/0022-3719/7/1/016.

CC

Appendix

Summarized MATLAB codes to form the Hamiltonian matrices

```
%% BNNR_Extended(BNNRtype, BNNRwidth, BNNRlength)
%% Initialization
clf,
global bandgapBNNR,
%% Device Specifications
% Type 1: ABNNR, Type 2: ZBNNR
% Valid width for ABNNR, n = 3, 4, 5 ...
% Valid width for ZBNNR, n = 2, 3, 4 ...

type = 2,
NW = 10,            %Width of BNNR
NL = 3,             %Length of BNNR
a = 2*NW*NL,
z = 3,              %Edge perturbation strength, range from -3 eV until +3 eV
Eb = -6.64,
En = -11.47,

t = -3.01834,       % Tight-binding energy between boron and nitride atoms
etaDOS1 = 1i*1e-1,  % Small imaginary number for DOS1 calculation
etaDOS2 = 0.0259,   % Small real number for DOS2 calculation, kT(eV) @ 300K

q = 1.6e-19,
hbar = 1.06e-34,
h = 2*pi*hbar,
m = 9.1e-31,
zplus=1i*1e-3,

errmax = 1e-3,

p = linspace(1,50,50),

%% Hamiltonian Setup
if type == 1     %ABNNR selected

    %Construct alpha for Armchair BNNR
    alpha = t*diag(ones(1,(2*NW)-1),1)+t*diag(ones(1,(2*NW)-1),-1),
    alpha(1,2*NW) = t,
    alpha(2*NW,1) = t,

    if mod(NW,2) == 0
        %Alpha matrix, loop iteration count, for even width ABNNR
        ABNNR_alpha_i = (NW-2)/2,
        %Extra step taken to delete non-existent bonds from alpha matrix
        alpha((NW+2),(NW+3)) = 0,
        alpha((NW+3),(NW+2)) = 0,
    else
        %Alpha matrix, loop iteration count, for odd width ABNNR
        ABNNR_alpha_i = (NW-3)/2,
    end

    %Inserting extra parameters to complete ABNNR alpha matrix
    for ABNNR_alpha_c = 0:ABNNR_alpha_i-1
        alpha(5+2*ABNNR_alpha_c , 2*NW-2*ABNNR_alpha_c) = t,
        alpha(2*NW-2*ABNNR_alpha_c , 5+2*ABNNR_alpha_c) = t,
    end
    for w = 1:(NW*2)
        if mod(w,2) == 0
            alpha(w,w)=-11.47,
        else
            alpha(w,w)=-6.64,
        end
    end
    %Construct beta matrix for Armchair BNNR

    beta_new = zeros(2*NW,2*NW),   %Initialize beta matrix
    alpha_new = zeros(2*NW,2*NW), %Initialize alpha matrix

    if mod(NW,2) == 0
        %Beta matrix, loop iteration count, for even width ABNNR
        ABNNR_beta_i = (NW/2),
    else
        %Beta matrix, loop iteration count, for odd width ABNNR
        ABNNR_beta_i = (NW-1)/2,
    end

    %Insert coupling terms between ABNNR unit cells in length direction
    for ABNNR_beta_c = 1:ABNNR_beta_i
        ABNNR_beta_row = 2*ABNNR_beta_c + 2,
        ABNNR_beta_col = 2*NW - (2*ABNNR_beta_c - 3),

        if ABNNR_beta_c == 1
            ABNNR_beta_col = 1,
        end

        beta(ABNNR_beta_row, ABNNR_beta_col) = t,
    end

else     %ZBNNR selected

    %Construct alpha for Zigzag BNNR
    alpha = t*diag(ones(1,(2*NW)-1),1)+t*diag(ones(1,(2*NW)-1),-1),
    for w = 1:(NW*2)
        if mod(w,2) == 0
            alpha(w,w)=En,
        else
            alpha(w,w)=Eb,
        end
    end
    %Contruct beta matrix for Zigzag BNNR

    beta_new = zeros(2*NW,2*NW), %Initialize beta matrix
    alpha_new = zeros(2*NW,2*NW), %Initialize alpha matrix

    %Insert coupling terms between ZBNNR unit cells in length direction
    for ZBNNR_beta_c = 1:NW
        if ZBNNR_beta_c == 1
            ZBNNR_beta_row = 1,
            ZBNNR_beta_col = 2,
        else
            if mod(ZBNNR_beta_c,2) == 0
                %Current ZBNNR loop iteration count is even
                ZBNNR_beta_row = ZBNNR_beta_row + 3,
                ZBNNR_beta_col = ZBNNR_beta_col + 1,
            else
                %Current ZBNNR loop iteration count is odd
                ZBNNR_beta_row = ZBNNR_beta_row + 1,
                ZBNNR_beta_col = ZBNNR_beta_col + 3,
            end
        end

        beta(ZBNNR_beta_row, ZBNNR_beta_col) = t,
    end

end

%Generate full device Hamiltonian (Length dependent)
H = kron(diag(ones(1,NL)),alpha)+kron(diag(ones(1,NL-1),1),beta)+kron(diag(ones(1,NL-1),-1),beta'),
fprintf(1,'Device Hamiltonian generated!\n\n'),
```